

Systematic 2.5 D resistive MHD simulations with ambipolar diffusion and Hall effect for fast magnetic reconnection

Gabriela Landinez^a, Fabio D. Lora-Clavijo^a

^aUniversidad Industrial de Santander, A. A. 678, Bucaramanga, 680002, Santander, Colombia

Abstract

In this work, we explore the possibility of the Hall effect and ambipolar diffusion as a mechanism for fast reconnection. The reconnected flux of our resistive and resistive+Hall simulations replicates the GEM results. Furthermore, we investigate, for the first time, the effect of ambipolar diffusion in the GEM. The reconnected flux of the resistive+ambipolar and resistive+Hall+ambipolar simulations showed increases of up to 75% and 143%, respectively, compared to the resistive and resistive+Hall simulations, showing that ambipolar diffusion contributes significantly to the reconnected flux. Our second scenario has a magnetic Harris field without perturbations but with an out-of-plane component, known as a guide field. We found that the reconnection rate increased faster with ambipolar diffusion, reaching values close to 0.1 for the resistive+Hall+ambipolar simulation followed by the resistive+Hall. These two simulations achieved the highest kinetic energy, implying more efficient energy conversion during reconnection.

Keywords: magnetic reconnection, Hall MHD, ambipolar diffusion, numerical simulations, numerical methods

1. Introduction

Magnetic reconnection is a topological rearrangement of the magnetic field that converts magnetic energy into plasma energy (Zweibel and Yamada, 2009). This process is usually described in terms of a change in the connectivity of the field lines, also known as the magnetic field topology, which allows the release of magnetic energy stored in the system. The Ohmic resistivity is responsible for this release, causing the plasma frozen-in-flux condition to be violated in the diffusion zone, where breaking and reconnection of magnetic field lines occur (Priest and Forbes, 2000; Bittencourt, 2013). Magnetic reconnection takes place in different plasmas, spanning from laboratory to astrophysical environments, is responsible for the different mechanisms of particle acceleration, the main driver of space weather (Priest and Forbes, 2000; Birn et al., 2012) and astrophysical phenomena, such as geomagnetic storms. To understand the energy conversion associated with these phenomena, it is essential to know the rate at which magnetic reconnection occurs (Comisso and Bhattacharjee, 2016). For example, the amplitude of geomagnetic disturbances can be controlled by the rate of magnetic reconnection (Nakamura et al., 2018), which provides information about how fast the process occurs, how much magnetic flux is reconnected, and how much magnetic energy becomes kinetic energy that accelerates the plasma (Hesse and Cassak, 2020). For these reasons, the magnetic reconnection rate has been studied observationally, experimentally, theoretically, and numerically. Nowadays, it is known from numerical simulations and satellite observations that the normalized reconnection rate is about 0.1 in many systems (Cassak et al., 2017; Hesse and Cassak, 2020), a much larger value than that predicted by the classical model of Sweet

(Sweet, 1958b,a) and Parker (Parker, 1957, 1963). However, despite years of effort and first-principles theories (Liu et al., 2022; Goodbred and Liu, 2022), a complete theoretical understanding has not been achieved. The above suggests that those classical models are insufficient to capture all the relevant processes during reconnection, probably because the physical mechanisms for fast reconnection are challenging to study through theoretical means (Malyskin and Zweibel, 2011).

The key to explaining a value of 0.1 may lie in studying the particle decoupling caused by the Hall effect, or in other physical phenomena beyond the single-fluid magnetohydrodynamic (MHD) approximation, like ambipolar diffusion. The GEM reconnection challenge (Birn et al., 2001) looked into that and verified that all their models with the Hall effect had similar reconnection rates, but later other simulations (Karimabadi et al., 2004; Bessho and Bhattacharjee, 2005, 2007) showed that reconnection also has a similar rate without this effect. However, most of these works are not concerned with partially ionized plasmas. According to Malyskin and Zweibel (2011), in a weakly ionized plasma with significant interaction between ions and neutrals, fast reconnection is triggered by the Hall effect at considerably lower Lundquist number values compared to scenarios with fully ionized plasma. These conditions for fast reconnection are satisfied in molecular clouds, where another effect could play a key role: the ambipolar diffusion, which is extremely important in astrophysics and contributes significantly to events of interstellar medium heating (Falgarone et al., 2015; Zweibel, 2015). So far, simulations have shown that ambipolar diffusion causes thinning of the current sheet, favouring rapid reconnection rates (Ethan and Lazarian, 1999; Heitsch and Zweibel, 2003; Ni et al., 2015). However, the direct effect of ambipolar diffusion on the reconnection rate has yet to be

well studied in the Earth’s magnetotail. While the literature on the value 0.1 for partially ionized plasmas is limited, numerical kinetic simulations suggest that magnetic reconnection rates can approach this value (Jara-Almonte et al., 2019). Although research on magnetic reconnection in partially ionized plasmas is less extensive, a multitude of astrophysical environments, including the lower solar atmosphere, comet tails, protoplanetary nebulae, and disks around young stellar objects, are filled with partially ionized plasmas. This motivates further investigation into the underlying mechanisms driving fast reconnection and the conditions under which it can occur in these environments.

Even in the presence of neutrals, all plasma components can be assumed to be strongly coupled by collisions, and the single fluid remains adequate. In many cases, however, collisions between particles are not sufficient to fully couple all species in a plasma. For example, in diffusion regions where magnetic reconnection occurs, the single-fluid approximation is no longer valid: ions are decoupled from the magnetic field and no longer move with electrons. Similarly, there are regions where the neutral gas in a plasma separates from the charged particles. This gives rise to relative velocities that manifest themselves as non-ideal processes, such as the Hall effect and ambipolar diffusion (Khomenko and Collados, 2012). Fortunately, even when the plasma is modelled as a single fluid, it is possible to adopt an approach to deal with the effects produced by the interaction between its species. This approach, instead of including more fluids in the system, relies on the use of a generalized Ohm’s law, whose additional terms contain the necessary information to describe a plasma where the different species are not strongly coupled.

With the above motivation, we address the problem of magnetic reconnection rate by performing a systematic comparison of simulations. We take a single-fluid approach with terms associated with the Hall effect and ambipolar diffusion in the resistive MHD equations. We do this to determine the effect of both phenomena on the behaviour of magnetic reconnection, in particular on the amount of reconnected flux and the reconnection rate. All numerical simulations are obtained by implementing and modifying subroutines in the MAGNUS code (Navarro et al., 2017). The paper is structured as follows. In section 2 we present the resistive MHD equations with the Hall effect and ambipolar diffusion, which are included in the equations through Ohm’s law. In section 3 we give a brief description of MAGNUS and the inclusion of both effects in the code. Then, in section 4 we perform the GEM benchmark test for the Hall effect. To our knowledge, no one has used the GEM to study the effect of ambipolar diffusion on the reconnected flux, so in section 5 we present simulations with ambipolar diffusion using the GEM model too. In section 6 we present the results for another simple current sheet model with guide field, in which we measure reconnection rates, magnetic and kinetic energies, and fluxes related to the energy transport equation. Finally, in section 7 we summarize the main conclusions.

2. MHD equations for a conducting fluid with Hall and ambipolar terms

As mentioned above, we take a single-fluid approach with Hall and ambipolar diffusion terms in the resistive MHD equations. The MHD model describes low-frequency interactions between conducting fluids and electromagnetic fields, i.e. motions where $u^2/c^2 \ll 1$, where u is the characteristic fluid velocity and c is the speed of light (Schnack, 2009).

2.1. Ohm’s law

Ohm’s law couples the dynamics of the fluid and the electromagnetic fields, taking into account non-ideal MHD processes beyond the ohmic resistance. For a reference frame in which the fluid moves with velocity \mathbf{u} , Ohm’s law reads as follows (Bittencourt, 2013; Ballester et al., 2018)

$$\mathbf{E} + \mathbf{u} \times \mathbf{B} = \eta \mathbf{j} + \eta_H (\mathbf{j} \times \mathbf{B}) - \eta_A [(\mathbf{j} \times \mathbf{B}) \times \mathbf{B}], \quad (1)$$

where η is the ohmic resistivity, η_H is the Hall coefficient, and η_A is the ambipolar diffusion coefficient. The coefficients are defined as

$$\eta_H = \frac{1}{ne}, \quad \eta_A = K_A \cdot \frac{1}{\rho^2 \sqrt{T}}, \quad (2)$$

where n is the number density, e is the electron charge, ρ is the plasma density, and T is the temperature. K_A is a parameter that controls the effect of the ambipolar term in our simulations and depends on the collision frequencies between particles and the physical conditions of the plasma (Viganò et al., 2019). For example, K_A is inversely related to the degree of ionization, so for a fully ionized plasma, K_A becomes zero and we do not have ambipolar diffusion. Ohm’s law is often derived from the electron momentum equation under simplifying assumptions, such as neglecting electron inertia, gravity acting on electrons, and assuming that currents vary much more slowly in time than hydrodynamic processes (Zaqarashvili et al., 2011). Additionally, strong couplings, which are sometimes broken in partially ionized plasmas (Brandenburg and Zweibel, 1994; Brandenburg and Zweibel, 1995), are often assumed. For a detailed discussion of Ohm’s law in multi-component partially ionized plasmas, see (Khomenko et al., 2014). In this research, we focus specifically on analyzing the impact of Hall terms and ambipolar diffusion on the plasma dynamics associated with magnetic reconnection phenomena.

2.1.1. Hall effect

The Hall effect refers to the appearance of an electric field due to charge separation in a conductor. In plasma, the separation occurs as a consequence of decoupling between ions and electrons that takes place in the diffusion region, where a multi-scale structure is developed based on the characteristic lengths of each species.

The Hall term arises from the separation of electron and ion motions in the plasma. In the generalized Ohm’s law, this term captures the dynamics of the magnetic field at scales smaller than the ion inertial length. Including the Hall term allows for a faster reconnection rate than predicted by classical MHD. This

is essential for explaining the rapid energy release observed in many astrophysical and laboratory plasmas. The Hall term leads to the formation of quadrupolar magnetic fields around the reconnection site. These structures are key observational signatures in both simulations and experiments.

Given an initial antiparallel magnetic field as the one in Figure 1, the term $\mathbf{j} \times \mathbf{B}$ implies the appearance of electric fields in the xy plane, where reconnection occurs. To understand the dynamics of ions and electrons influenced by these electric fields and the appearance of the quadrupole field, a characteristic signature of Hall reconnection, the reader may refer to the physical picture made by Uzdensky and Kulsrud (2006). Their description provides a clear example of how currents induced by the Hall effect may affect the structure of the initial current sheet as well as the magnetic field and its evolution (Morales, 2020).

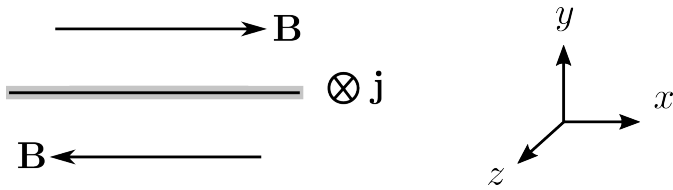


Figure 1: Simple diagram of a current sheet. The magnetic field is located in the xy plane and the current sheet in the xz plane is oriented towards the $-z$ axis.

2.1.2. Ambipolar diffusion

Ambipolar diffusion affects the transport of magnetic flux and can lead to the decoupling of magnetic fields from the bulk plasma. This decoupling is crucial for understanding the reconnection process in environments where neutrals are present.

Ambipolar diffusion also produces the appearance of electric fields, this time due to decoupling between neutrals and charged particles (Zweibel, 2015). The ambipolar term $(\mathbf{j} \times \mathbf{B}) \times \mathbf{B}$ generates electric fields in the xz plane of Figure 1, as a consequence it affects the perpendicular currents to the reconnection plane. According to Morales (2020), this implies that ambipolar diffusion cannot produce magnetic reconnection. However, it can relax the magnetic field configuration by reducing the magnetic energy, which is then converted to heat by a dissipation process.

Ambipolar diffusion influences the reconnection rates by modifying the resistivity in the plasma. Depending on the local plasma conditions, this can either enhance or suppress the reconnection rate. In astrophysical contexts, such as star formation and the evolution of molecular clouds. Understanding its impact is necessary for realistic modelling of these processes.

Although the Hall effect generates currents in the plane where reconnection occurs, it does not contribute directly to reconnection because it continues to freeze the magnetic field in the electron flow (Priest and Forbes, 2000). In fact, both effects, unlike ohmic resistance, preserve the magnetic field topology and do not trigger reconnection. However, they can promote its occurrence and affect its rate with effects such as current sheet thinning and plasmoid formation (Nóbrega-Siverio et al., 2020; Zweibel, 2015). Including both terms in the generalized Ohm's

law lead to better predictions of reconnection rates, energy release, and the overall behaviour of plasma in both astrophysical and laboratory settings.

Finally, it is important to clarify that the appearance of electric fields in the plane where reconnection occurs, or in its perpendicular plane, will change depending on the configuration adopted, e.g. if a guide field is used, the z component of the magnetic field must be considered. Figure 1 is only used to illustrate a simple and specific configuration.

2.2. Transport equations

When the plasma, which may contain ions, electrons, and neutrals, is considered as a single conducting fluid, the transport equations for each species are replaced by transport equations for the whole plasma, meaning that variables such as density and velocity for each species are replaced by average values (Bittencourt, 2013). In conservative form, the macroscopic transport equations for a conducting fluid are

$$\frac{\partial \rho}{\partial t} + \nabla \cdot (\rho \mathbf{u}) = 0, \quad (3)$$

$$\frac{\partial \rho \mathbf{u}}{\partial t} + \nabla \cdot \left(\rho \mathbf{u} \mathbf{u} - \frac{1}{\mu_0} \mathbf{B} \mathbf{B} + P \mathbf{I} \right) = 0, \quad (4)$$

$$\frac{\partial E}{\partial t} + \nabla \cdot \left\{ (E + P) \mathbf{u} - \frac{1}{\mu_0} (\mathbf{B} \cdot \mathbf{u}) \mathbf{B} + \frac{1}{\mu_0} [B^2 \mathbf{u}_H - (\mathbf{B} \cdot \mathbf{u}_H) \mathbf{B}] + \frac{1}{\mu_0} (B^2 \mathbf{u}_A) \right\} = -\nabla \cdot \left(\frac{\eta}{\mu_0} \mathbf{j} \times \mathbf{B} \right), \quad (5)$$

where \mathbf{u}_H and \mathbf{u}_A are velocities associated with the Hall effect and the ambipolar diffusion, defined as

$$\mathbf{u}_H = -\eta_H \mathbf{j}, \quad \mathbf{u}_A = \eta_A (\mathbf{j} \times \mathbf{B}). \quad (6)$$

The total pressure P is defined as

$$P = p + \frac{B^2}{2\mu_0}, \quad (7)$$

the sum of fluid pressure p and the magnetic pressure $B^2/2\mu_0$. The total energy density E is given by the sum of the kinetic, magnetic and internal energy densities, that is

$$E = \frac{1}{2} \rho u^2 + \frac{1}{2\mu_0} B^2 + \rho e, \quad (8)$$

here e is the system's internal energy and is related to pressure by the equation of state

$$p = (\gamma - 1) \rho e, \quad (9)$$

where γ is the adiabatic index. The equations (3), (4) and (5) correspond to the transport equations for mass, momentum and energy. To obtain them, no gravitational force is assumed, viscosity and heat flow are neglected.

2.3. Evolution equations for the electromagnetic fields

Evolution equations for \mathbf{E} and \mathbf{B} are given by Faraday's and Ampère-Maxwell's laws,

$$\nabla \times \mathbf{E} = -\frac{\partial \mathbf{B}}{\partial t}, \quad (10)$$

$$\nabla \times \mathbf{B} = \mu_0 \mathbf{j}, \quad (11)$$

where the displacement current term in equation (11) is neglected due to the low-speed approximation. Also, at all times it must be guaranteed that

$$\nabla \cdot \mathbf{B} = 0, \quad (12)$$

which also guarantees the absence of magnetic monopoles. Finally, Faraday's law can be rewritten using Ohm's law to obtain the induction equation

$$\frac{\partial \mathbf{B}}{\partial t} + \nabla \cdot (\mathbf{u}\mathbf{B} - \mathbf{B}\mathbf{u}) + \nabla \cdot (\mathbf{u}_H \mathbf{B} - \mathbf{B}\mathbf{u}_H) + \nabla \cdot (\mathbf{u}_A \mathbf{B} - \mathbf{B}\mathbf{u}_A) = -\nabla \times \eta \mathbf{j}. \quad (13)$$

With equations (12) and (13), the system of equations (3)-(5) is closed and we can proceed with the numerical methods used to solve it.

3. Numerical methods: MAGNUS code

MAGNUS (Navarro et al., 2017) is the Newtonian version of the relativistic code CAFE (Lora-Clavijo et al., 2015). It solves the resistive MHD equations and has been used mainly to study wave propagation in the solar atmosphere. Some of the scenarios that have been simulated with MAGNUS are: the emerging plasma blob in a solar coronal hole (Navarro et al., 2019), the thermal conduction effects on the formation of tadpole-like jets in the solar chromosphere (Navarro et al., 2021), and the propagation of torsional Alfvén waves in a stratified solar atmosphere (Wandurraga et al., 2021). More recently, an adaptation of MAGNUS has been used to model the propagation of PS-V seismic waves (Landinez et al., 2021).

The code solves the system of equations in a uniform grid using the method of lines, whose main idea is to replace the spatial derivatives by algebraic approximations (Schiesser and Griffiths, 2009). Once this is done, any integration method can be used to compute a solution. In MAGNUS, the algebraic approximation of the right-hand side of the equations is done using the finite volume method in combination with the HLLE approximate Riemann solver, which uses different slope limiters. The time integration can be done with different integrators of the Runge-Kutta family implemented in MAGNUS. In particular, we use the MC beta limiter with $\beta = 1.2$ and a TVD second-order Runge-Kutta in all simulations.

The finite volume discretization of the MHD equations, including Hall and ambipolar terms, modifies the induction equation and the total energy density equation. We found that it is not possible to consider the Hall term as an additional source term, therefore it is necessary to add new terms to the numerical fluxes.

3.1. Hall and ambipolar corrections to the fluxes

With the velocities \mathbf{u}_H and \mathbf{u}_A , the energy and induction equations can be rewritten in coordinates as

$$\begin{aligned} \frac{\partial E}{\partial t} = & -\frac{\partial}{\partial x_j} \left[(E + P)u_j - \frac{1}{\mu_0} (\mathbf{B} \cdot \mathbf{u}) B_j \right] \\ & - \frac{\partial}{\partial x_j} \left[B^2 u_j^H - (\mathbf{B} \cdot \mathbf{u}^H) B_j \right] \\ & - \frac{\partial}{\partial x_j} \left(B^2 u_j^A \right) - \left[\nabla \cdot \left(\frac{\eta}{\mu_0} \mathbf{j} \times \mathbf{B} \right) \right]_j, \end{aligned} \quad (14)$$

$$\begin{aligned} \frac{\partial B_i}{\partial t} = & -\frac{\partial}{\partial x_j} (u_j B_i - B_j u_i) - \frac{\partial}{\partial x_j} (u_j^H B_i - B_j u_i^H) \\ & - \frac{\partial}{\partial x_j} (u_j^A B_i - B_j u_i^A) - [\nabla \times \eta \mathbf{j}]_i. \end{aligned} \quad (15)$$

The magnetic permeability μ_0 does not appear in the above equations because MAGNUS solves the dimensionless system of equations.

The first three terms on the right-hand side of both equations are fluxes, while the others are source terms. Since MAGNUS already solves the resistive MHD equations, only the second and third terms in parentheses need to be added to the fluxes of each equation. With the finite volume method, the equations are discretized as

$$\begin{aligned} \frac{d\mathbf{U}_{(i,j,k)}}{dt} = & -\frac{\mathbf{F}_{(i+1/2,j,k)}^x - \mathbf{F}_{(i-1/2,j,k)}^x}{\Delta x} - \frac{\mathbf{F}_{(i,j+1/2,k)}^y - \mathbf{F}_{(i,j-1/2,k)}^y}{\Delta y} \\ & - \frac{\mathbf{F}_{(i,j,k+1/2)}^z - \mathbf{F}_{(i,j,k-1/2)}^z}{\Delta z} + \mathbf{S}_{(i,j,k)}, \end{aligned} \quad (16)$$

where \mathbf{U} is the state vector, \mathbf{F}^i the vector of fluxes along each direction¹, and \mathbf{S} the vector of source terms. In MAGNUS, each vector of fluxes is calculated as

$$\mathbf{F}_{i\pm 1/2,j,k} = \mathbf{F}_{i\pm 1/2,j,k}^{HLL E} + \mathbf{F}_{i\pm 1/2,j,k}^H + \mathbf{F}_{i\pm 1/2,j,k}^A, \quad (17)$$

where $F^{HLL E}$ is the numerical flux for the MHD part, calculated using the HLLE High-Resolution Shock Capturing method. F^H and F^A are the fluxes due to Hall and ambipolar terms, both computed in different subroutines and then added to the other fluxes computed with the HLLE scheme along each spatial direction. Equation (17) is analogous for $F_{i,j\pm 1/2,k}$, $F_{i,j,k\pm 1/2}$.

To compute the Hall and ambipolar velocities, which appear in (14) and (15), we need the magnetic field and the current density evaluated at the intercell. Since the current density is given by $\mathbf{j} = (\nabla \times \mathbf{B})/\mu_0$, we need the spatial derivatives of the magnetic field. For the latter, some authors propose schemes where the normal derivatives are computed differently from the tangential derivatives (see Tóth et al. (2008) and Strumik and Stasiewicz (2017)). However, we compute the derivatives of

¹By using 1/2 in one of the subindexes of the triplet (i, j, k) , we denote a face between cells in a given direction. For example, The subindex $(i+1/2, j, k)$ represents the face between cells in i direction, that is, the face between (i, j, k) and $(i+1, j, k)$.

the magnetic field along each direction using a second-order finite-difference scheme. At each of the nodes, the derivatives are numerically approximated using forward, backwards, and central finite differences. Once this is done, the Hall and ambipolar velocities can be obtained at each point in the numerical grid. We then use the averaged variables

$$(u^H)_{i+1/2,j,k} = \frac{(u^H)_{i,j,k} + (u^H)_{i+1,j,k}}{2}, \quad (18)$$

$$(u^A)_{i+1/2,j,k} = \frac{(u^A)_{i,j,k} + (u^A)_{i+1,j,k}}{2}, \quad (19)$$

to calculate the velocities at the intercell. The same is done for $(u^H)_{i,j+1/2,k}$, $(u^H)_{i,j,k+1/2}$, $(u^A)_{i,j+1/2,k}$ y $(u^A)_{i,j,k+1/2}$ and also for each component of the magnetic field in equations (14) and (15).

3.2. Time-step modification

Following the Courant-Friedrichs-Levy condition, the time step in MAGNUS is chosen as

$$\Delta t = C_{CFLL} \times \min \left(\frac{\Delta x}{|\lambda_{ijk}^{n,x}|}, \frac{\Delta y}{|\lambda_{ijk}^{n,y}|}, \frac{\Delta z}{|\lambda_{ijk}^{n,z}|} \right), \quad (20)$$

where the Courant-Friedrichs-Levy parameter C_{CFLL} must be less than or equal to 1, and $\lambda_{ijk}^{n,d}$ is the velocity of the fastest wave propagating in some d direction at a time level n (Navarro et al., 2017), so that the time step adapts at each level.

In the presence of Hall and ambipolar terms, some modifications are required. To do this, we performed a dimensional analysis of each of these terms in the induction equation. For the Hall term, we have

$$\frac{B_o}{t_o} = \eta_H \frac{j_o B_o}{x_o} = \eta_H \frac{B_o^2}{x_o^2}, \quad (21)$$

therefore

$$t_o = \frac{x_o^2}{B_o \eta_H} = \frac{x_o}{\frac{B_o \eta_H}{x_o}}. \quad (22)$$

It is clear that the denominator of the last fraction corresponds to some velocity. With this is defined a new velocity

$$\lambda_H = u + c_f + C \frac{B_o \eta_H}{x_o}, \quad (23)$$

where u is the fluid velocity and c_f is the fast magnetosonic velocity. According to Tóth et al. (2008), it is not necessary to include the exact speed of the modes introduced by the Hall effect, but a reduced speed can be used to guarantee the stability of the simulations. In this case, C is a constant that allows defining a reduced or extended speed of the Hall term. Thus, there is freedom in the choice of C that allows to better adapt the time step depending on the physical system to be simulated.

At each time level MAGNUS evaluates the speed λ_H at all points in the domain and chooses the largest. Then, the time step is calculated as

$$\Delta t_H = C_{CFLL} \times \left(\frac{\Delta x}{\lambda_{H,ijk}^{n,x}} + \frac{\Delta y}{\lambda_{H,ijk}^{n,y}} + \frac{\Delta z}{\lambda_{H,ijk}^{n,z}} \right). \quad (24)$$

The same is done with the ambipolar term, for which

$$\lambda_A = u + c_f + \frac{B_o^2 \eta_A}{x_o}, \quad (25)$$

and

$$\Delta t_A = C_{CFLL} \times \left(\frac{\Delta x}{\lambda_{A,ijk}^{n,x}} + \frac{\Delta y}{\lambda_{A,ijk}^{n,y}} + \frac{\Delta z}{\lambda_{A,ijk}^{n,z}} \right). \quad (26)$$

In the end, MAGNUS chooses the smallest time step between (20), (24) and (26).

3.3. Scaling and Nondimensionalization

As mentioned above, MAGNUS solves the dimensionless system of equations. Therefore, the dimensionless equations are the ones that evolve. Then the dimensionless quantities that result from the system's evolution can be scaled with quantities that do have dimensions and depend on the simulated physical system.

In the code, this is done by dividing each physical quantity by characteristic quantities of the system such as l_a , ρ_a , u_a and constants such as the magnetic permeability μ_0 . Including the Hall and ambipolar terms in the code makes it necessary to determine expressions for η_{Ha} and η_{Aa} .

4. GEM reconnection challenge

After the implementation of the Hall and ambipolar term in the MAGNUS code was done, we proceeded with the Geospace Environmental Modeling (GEM) reconnection challenge (Birn et al., 2001). The analytical solution to this problem is not known, but since its publication, several authors have reproduced their results, which is why it is often used as a benchmark test (Tóth et al., 2008; Strumik and Stasiewicz, 2017).

First, we use the GEM as a numerical test to verify the implementation of the Hall term in MAGNUS. For the test, the system starts from rest with a magnetic field whose components are defined as

$$B_x = \tanh(2z) + \delta B_x, \quad (27)$$

$$B_z = \delta B_z, \quad (28)$$

$$B_y = 0. \quad (29)$$

The perturbations δB_x and δB_z are defined as

$$\delta B_x = \frac{0.05\pi}{L_z} \cos\left(\frac{2\pi x}{2L_x}\right) \sin\left(\frac{\pi z}{2L_z}\right), \quad (30)$$

$$\delta B_z = \frac{0.1\pi}{L_x} \sin\left(\frac{2\pi x}{2L_x}\right) \cos\left(\frac{\pi z}{2L_z}\right). \quad (31)$$

The initial density is

$$\rho = 1.2 - [\tanh(2z)]^2, \quad (32)$$

and the pressure is $p = \rho/2$. In all simulations we set the resistivity to $\eta = 0.005$. In the resistive+Hall simulations, the normalized ion mass per charge is set to 1.0, so that $\eta_H = 1/\rho$.

In both cases, resistive and resistive+Hall, the simulation box is $[-L_x, L_x] \times [-L_z, L_z] \times [-L_y, L_y]$, where $L_x = 12.8$, $L_z = 6.4$ and $L_y = 0.2$. In this volume, the equations are discretized in a three-dimensional numerical grid with $N_x = 64$, $N_z = 128$ and $N_y = 4$. The boundary conditions are periodic in x , inflow in z and outflow in y .

Figure 2 shows the reconnected flux of resistive and resistive+Hall simulations. In both, the flux is calculated at each time step as

$$\text{Reconnected flux} = \int_{N_x/2}^{N_x} B_z(x, N_y/2, N_z/2) dx. \quad (33)$$

With the Hall effect, the reconnected flux reaches a value of 3.3, about six times larger than in the simulation with resistivity alone, where the reconnected flux reaches a value of 0.5. This result is in qualitative and quantitative agreement with those presented in GEM for MHD and Particle-In-Cell (PIC) simulations. For comparison see Figure 1 of Birn et al. (2001), at $t = 30$ the Hall MHD case reaches a reconnected flux of about 3.2. See the bottom panel of Figure 1 from Pritchett (2001), the reconnected flux reaches a value slightly above 3.0.

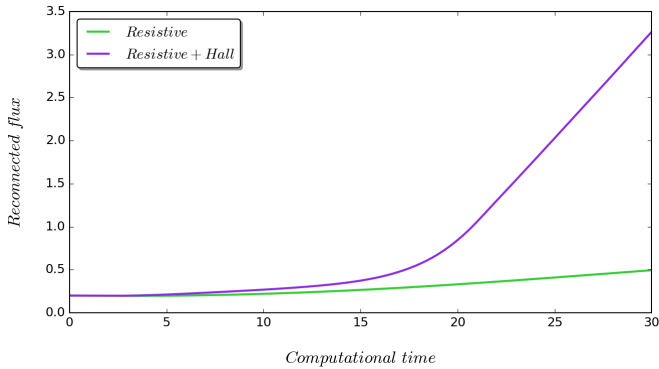


Figure 2: Testing results of the reconnected flux for the initial data of the GEM reconnection challenge.

These results are also consistent with those of other authors who have used GEM as a benchmark. For example, in the kinetic simulation of Schmitz and Grauer (2006) the curve reaches a value slightly above 3.0, similar to the MHD simulation of Tóth et al. (2008), both at time $t = 30$. This differs slightly from the results of Strumik and Stasiewicz (2017), whose MHD simulation reaches a value of 2.5, lower than the simulations mentioned above and the results shown in Figure 2. For the resistive case, the result presented in Figure 2 is also in agreement with those presented by Birn et al. (2001); Tóth et al. (2008); Strumik and Stasiewicz (2017).

5. Ambipolar diffusion in the GEM

Although the GEM was designed to study the Hall effect on magnetic reconnection, we use the same scenario to study the effect of ambipolar diffusion. To our knowledge, such a systematic study of simulations with ambipolar diffusion in the GEM

model has not been done before. In fact, ambipolar diffusion had been overlooked in the Earth's magnetotail.

We present two types of simulations: resistive+ambipolar and resistive+Hall+ambipolar. The Hall parameter remains unchanged, with the same value as in the previous section ($\eta_H = 1/\rho$). The ambipolar term, $\eta_A = K_A \cdot 1/\rho^2 \sqrt{T}$, is implemented with $T = p/\rho$. Three values of K_A are considered: 0.001, 0.005, and 0.01 (since K_A is inversely proportional to the degree of ionization, the latter value represents the less ionized case). These values were selected taking into account equation (22) from (Ni et al., 2015). These values physically correspond to values of η_A in the chromosphere. The code being dimensional allows for the straightforward use of these values without any issues.

Figure 3 shows the reconnected flux of the resistive simulation compared to the resistive+ambipolar cases. As can be seen, the reconnected flux grows with the value of K_A , obtaining an increase of about 7% for $K_A = 0.001$, 38% for $K_A = 0.005$, and 75% for $K_A = 0.01$, all percentages with respect to the resistive case. Comparing with figure 2, we see that the increase of the reconnected flux is much higher with the Hall effect than with the ambipolar diffusion, but the percentages indicate that the ambipolar diffusion also contributes to the reconnected flux. Furthermore, its increase could be higher if other values of K_A are considered. Figure 4 compares the reconnected flux of the resistive+Hall simulation with the resistive+Hall+ambipolar cases. For the case with $K_A = 0.01$, the reconnected flux grows faster until it reaches an increase of 143% (with respect to the resistive+Hall case) at time $t = 18$ and then remains approximately stationary until the end. This quasi-steady state of the reconnected flux seems to be caused by the appearance of a plasmoid in the centre of the domain at $t = 18$.

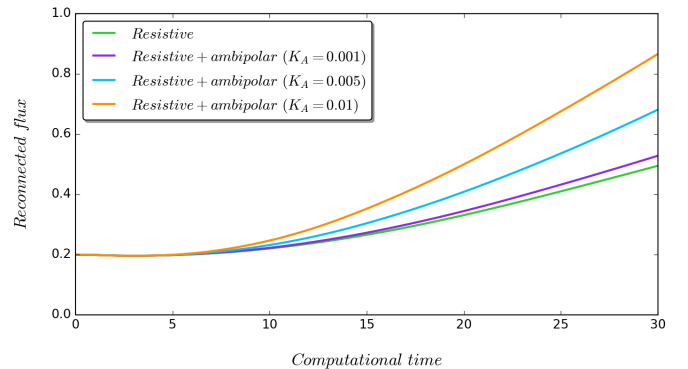


Figure 3: Reconnected flux for different values of the K_A parameter in the resistive+ambipolar simulations.

To illustrate the qualitative differences between some of the simulations carried out, Figure 5 shows the current density at time $t = 20$ for the four types of simulations: resistive, resistive+Hall, resistive+ambipolar, and resistive+Hall+ambipolar, using $K_A = 0.01$ for those that include the ambipolar term. For the resistive simulation (upper left panel), we observe an elongated current sheet of nearly the order of the global length scale,

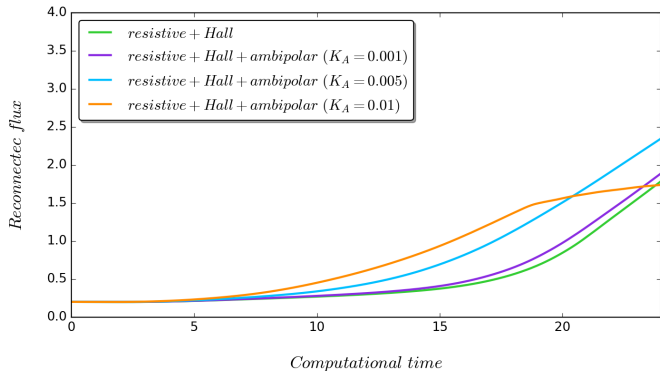


Figure 4: Reconnected flux for different values of the K_A parameter in the resistive+Hall+ambipolar MHD simulations.

as proposed by the model of Sweet-Parker. By including the ambipolar term (lower left panel) we observe a thinner current sheet, in agreement with the results of Ni et al. (2015), where the inclusion of ambipolar diffusion causes a rapid thinning of the current sheet in the solar chromosphere.

Together with the reconnected flux shown in Figure 3, these results support the fact that elongated current sheets result in low reconnection rates, which are inconsistent with the rate suggested by observations. For the resistive+Hall simulation (upper right panel), the diffusion region is much smaller as the current density is concentrated in an x-shaped region in the centre of the domain, a result consistent with the one presented by Strumik and Stasiewicz (2017). However, it differs from the one presented by Tóth et al. (2008), whose simulation with the Hall effect shows asymmetric behaviour, has two reconnection regions and a plasmoid, a result that is not obtained with MAGNUS for any time of the resistive+Hall simulation case. In fact, the combination of the Hall effect with ambipolar diffusion in the resistive+Hall+ambipolar case is the only one that produces the formation of a plasmoid (bottom right panel).

It is worth checking whether the plasmoid is due to insufficient resolution. For that, in Figure 6 we present the results of two more simulations with higher resolution: the first one with 128×256 and the second with 256×512 grid points. Both panels of Figure 6 show the same global morphology. Locally, the higher resolution panel reveals more detail, but the appearance of the plasmoid in the centre of the domain is consistent in simulations with different resolutions. Based on these results, we can confirm that the appearance of the plasmoid is not due to a numerical issue.

Concerning the formation of the plasmoid, we want to highlight the current sheet thinning caused by the ambipolar diffusion that can be seen in 5. We believe that the spatial scale reduction, attributed to the thinning of the current sheet characteristic of ambipolar diffusion, is likely crucial for bringing magnetic field lines close enough together to facilitate magnetic reconnection. Moreover, in a region of strong magnetic gradient, ambipolar diffusion can allow electrons to move faster than ions, which can cause the formation of thin current layers and then the possible appearance of instabilities in those

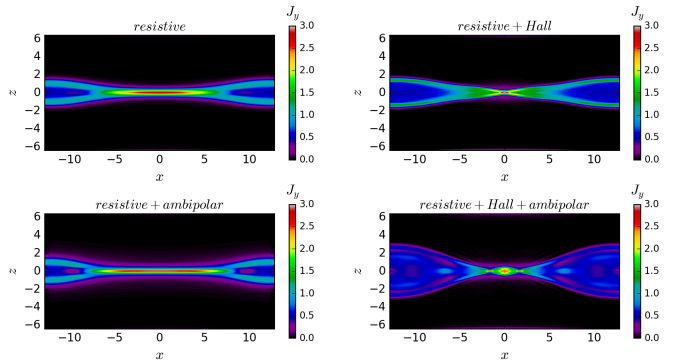


Figure 5: Out-of-plane component of the current density at time $t = 20$. The simulations with Hall effect and ambipolar diffusion have parameters $K_H = 1.0$ and $K_A = 0.01$.

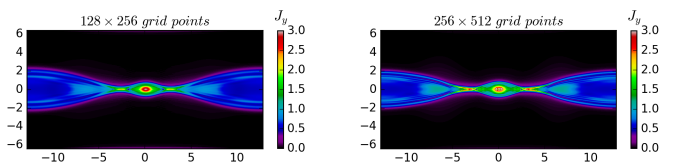


Figure 6: Out-of-plane component of the current density at time $t = 18$ with higher resolutions.

layers. These instabilities can evolve towards the formation of plasmoids.

We believe that the formation of the plasmoid in the simulation is facilitated by the combined effects. However, substantiating this claim requires a systematic study solely focused on plasmoid formation, demonstrating how these combined effects enhance the likelihood of plasmoid formation. It is crucial to emphasize that plasmoid formation cannot be attributed to a single phenomenon. Rather, it emerges from the interaction and dynamics of multiple factors. As noted by Singh et al. (2019), while the thinning of the current sheet plays an important role in plasmoid formation, it is influenced not only by this thinning but also by additional factors that collectively shape the overall dynamics of magnetic reconnection.

6. Current sheet with a guide-field

This second model attempts to simulate the process of magnetic reconnection from the formation of a current sheet. It also includes the presence of a guide field, that is, the non-reconnecting component of the magnetic field that is out-of-plane. This out-of-plane component is commonly used in solar flare simulations and plays an important role in determining key properties of reconnection, like the efficiency of particle acceleration (Dahlin et al., 2022). Unlike the GEM, in this model, we use initial data with constant density, constant pressure, and magnetic field without perturbations. This ensures that the current sheet is not formed at time zero and that the reconnected flux is zero. To trigger reconnection, we use spatially localized resistivity.

The system starts from rest with a magnetic field whose components are defined as (Shibata et al., 2022)

$$B_x = B \tanh(y/w), \quad (34)$$

$$B_y = 0, \quad (35)$$

$$B_z = B / \cosh(y/w), \quad (36)$$

being B_z the guide-field with $B = 3.92$ and $w = 0.5$. Density and initial pressure of the system are given by $\rho = 1.0$ and $p = 1.0$, and the localized resistivity is given by the function

$$\eta = \eta_0 \cdot \exp \left[- \left(\frac{\sqrt{y^2 + (x - h_\eta)^2}}{w_\eta} \right)^2 \right], \quad (37)$$

with $\eta_0 = 0.01$, $h_\eta = 15.0$ and $w_\eta = 1.0$. The computational domain is $[0, L_x] \times [-L_y/2, L_y/2] \times [-L_z/2, L_z/2]$ where $L_x = 30.0$, $L_y = 15.0$ and $L_z = 0.15$, with a numerical mesh with $N_x = 800$, $N_y = 400$ and $N_z = 4$. The boundary conditions are periodic in x , inflow in y and outflow in z .

With the previous specifications, four simulations are performed: resistive, resistive+Hall, resistive+ambipolar, and resistive+Hall+ambipolar. It is important to emphasize that in order to perform systematic simulations, the only thing that varies in each type of simulation is the presence or absence of the Hall effect and the ambipolar diffusion, which is controlled by the parameters η_H and η_A . The initial data, boundary conditions, computational domain, spatial resolution, and numerical methods are the same for all simulations. For the ambipolar coefficient, we used $K_A = 0.01$ and for the Hall coefficient, we set the normalized ion mass per charge to 0.2.

As mentioned above, the out-of-plane component of this model is also commonly used in solar flare simulations. That is one of the reasons why this second model is suitable for application to partially ionized plasmas, like the chromosphere, where ambipolar diffusion is a relevant phenomenon and could potentially impact its dynamics. In such instances, it is essential to select characteristic values for scaling the dimensionless outcomes derived from the computational code, so that the results may have dimensions according to the physical scenario. In our study, all quantities were kept dimensionless, meaning they were not scaled to fit a particular scenario. This approach allowed us to focus on assessing the potential impact and effects of the Hall and ambipolar diffusion terms on reconnection itself, rather than their applicability to a specific context.

6.1. Current sheet morphology

First, we examine the current sheet morphology at time $t = 12t_a$, where t_a is a characteristic time. Figure 7 shows the temperature distribution in the current sheet for each simulation. It can be seen that the current sheet centre is the hottest region, especially in the resistive and resistive+ambipolar cases. For the resistive+Hall and resistive+Hall+ambipolar simulations, the central region is not as hot, but we see heating at the extremes of the domain, particularly in the presence of the ambipolar term.

Regarding the plasma velocities, Figure 8 shows maps for the u_x component, where we can clearly see the presence of

two flows with opposite directions coming out of the central region. This indicates that the plasma is being accelerated out of the current sheet, one of the main consequences of reconnection. Therefore, this type of velocity diagram is characteristic of magnetic reconnection and is also consistent with the diagrams in the PIC simulations of Nakamura et al. (2018), which were performed to model a reconnection event detected by MMS. The different panels of figure 8 also show that the high-velocity regions are bigger in the presence of the Hall effect and ambipolar diffusion. Thus, both effects contribute to the acceleration of particles.

Finally, figure 9 shows maps for the u_y component. In the panels, we see that the plasma is moving toward the current sheet, with positive velocities in the lower region of the domain and negative velocities in the upper region. Towards the extremes of the domain, where the current sheet opens, this distribution of velocities changes: negative velocities are present in the lower region and positive in the upper region. This indicates that although the plasma enters the diffusion region, it is also expelled from it according to the scheme of magnetic reconnection. We can also see that the plasma regions with the highest velocities are located at the extremes of the current sheet. There, the colour distribution indicates that there are abrupt changes in both the magnitude and direction of the velocity. This type of behaviour can trigger turbulence and be another mechanism contributing to plasma acceleration (Price et al., 2016). Three-dimensional MHD simulations of Shibata et al. (2022) and Shen et al. (2022) investigate the dynamics of solar flares with a focus on the generation of turbulence. These studies identified regions characterized by turbulent flows, which may significantly influence electron acceleration within these areas. Additionally, they found self-organized structures in turbulent interface flare regions, resembling formations also seen in supernova remnants. Further investigation on this topic is essential for understanding the mechanisms behind substantial energy releases and events of particle acceleration.

6.2. Reconnection rate

In addition to telling us that the flux is being reconnected, the reconnection rate is associated with the energy released during the process.

The original model for determining the reconnection rate was proposed by Sweet (1958b,a) and Parker (1957, 1963), considering a diffusion region with length L , on the order of the global external length scale that occupies the entire boundary between opposing magnetic fields. According to this model, the dimensionless reconnection rate is given by: $v_i/v_{Ai} = 1/\sqrt{S}$, where v_i is the characteristic speed of entry of the field lines into the diffusion region, v_{Ai} is the Alfvén speed at the entry and S is the Lundquist number. In general, the Lundquist number is large for most astrophysical plasmas ($S \gg 10^6$). Consequently, the Sweet-Parker reconnection is too slow to explain phenomena such as geomagnetic storms (Birn and Priest, 2007).

Simulations and observations have reported a fast rate of 0.1, and smaller values cannot explain the rapid energy release that accelerates the plasma. Here the dimensionless reconnection rate is calculated as v/v_A , where v is the plasma velocity at the

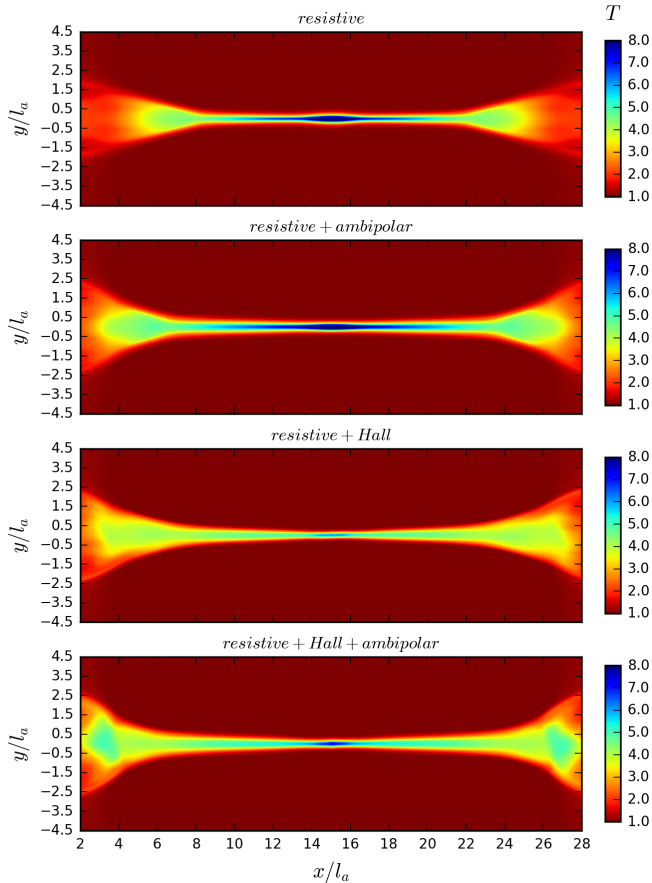


Figure 7: Temperature distribution at $t = 12t_a$. In all cases, the hottest region is found at the current sheet centre. For the resistive+Hall+ambipolar simulation, high heating is also observed at the extremes of the domain.

entrance of the diffusion region and v_A is the Alfvén velocity, also at the entrance (Priest and Forbes, 2000). Although it is impossible to determine the exact volume and location of the diffusion region, the localized resistivity in the centre of the region implies that we have a single reconnection site also located in the centre. Based on this, the entry to the diffusion region can be considered as the point located at $(N_x/2, N_{yi}, N_z/2)$, where N_{yi} is a point close to the line $y = 0.0$ ($N_y/2$), but not on it because there the magnetic field is zero. Thus, for all simulations, the reconnection rate is calculated as

$$\text{Reconnection rate} = \frac{v(N_x/2, N_{yi}, N_z/2)}{v_A(N_x/2, N_{yi}, N_z/2)}, \quad (38)$$

with N_{yi} on the line $y = 0.5$. The velocities are computed using only the components of the xy plane, that is, $v = \sqrt{v_x^2 + v_y^2}$ and $v_A = B/\sqrt{\rho}$ with $B = \sqrt{B_x^2 + B_y^2}$.

In Figure 10 we plot the reconnection rate as a function of time for the four types of simulations. The results show that when running systematic simulations, the resistive+Hall+ambipolar case reaches a reconnection rate of 0.1, followed by the resistive+Hall case. The Hall effect simulations show similar reconnection rates, implying that the Hall

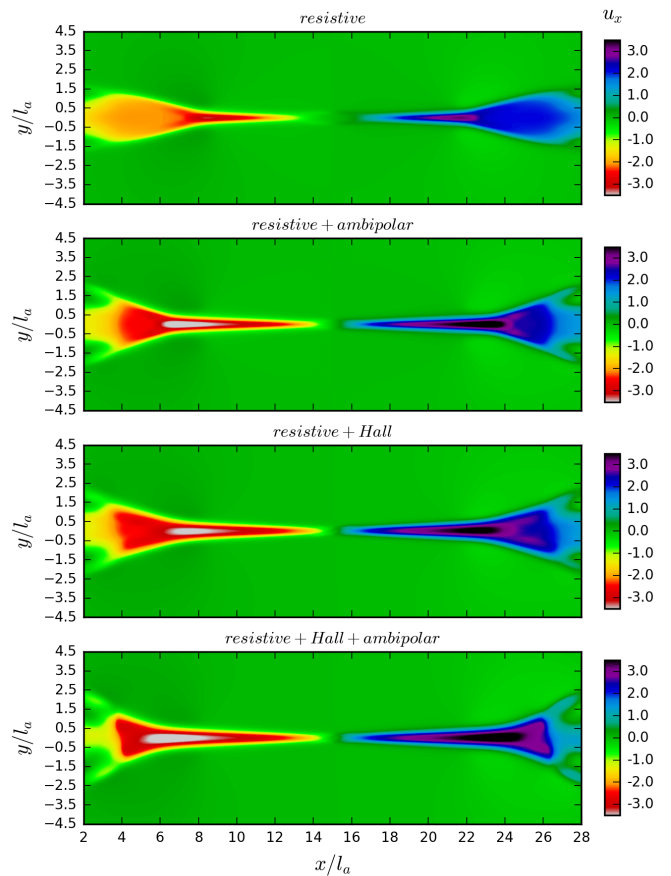


Figure 8: u_x velocity maps at $t = 12t_a$. All simulations exhibit two flows with opposite directions, a characteristic feature of magnetic reconnection. Moreover, the highest velocity regions widen in the presence of the Hall effect and ambipolar diffusion.

term is indeed important to obtain reconnection rates of 0.1. However, the results also show that the ambipolar term may play an important role in the reconnection rate. While the Hall effect dominates when reconnection rates are compared to the resistive case, it is the combination of the Hall effect and ambipolar diffusion that reaches a value of 0.1, comparable to what has been observed, for example, in the magnetosphere, where MMS values are 0.1 – 0.2 (Chen et al., 2017; Nakamura et al., 2018).

The ambipolar term also seems to influence the reconnection rate to increase faster, which is why the maximum rate appears earlier in the simulations with ambipolar diffusion, an effect also reported by other authors (see case C from model I and case F from model II in Figure 5 of Ni et al. (2015)). However, Ni et al. (2015) attribute this to the fact that ambipolar diffusion triggers plasmoid instability. Our results show that even without plasmoids, ambipolar diffusion has the effect of accelerating the reconnection process.

In our simulations, the Lundquist number is of the order of $S \sim 10^4$, which corresponds to a reconnection rate $S^{-1/2} \sim 0.01$ according to Sweet-Parker (as we mentioned above, the rate is calculated as $1/\sqrt{S}$). This shows that reconnection in our

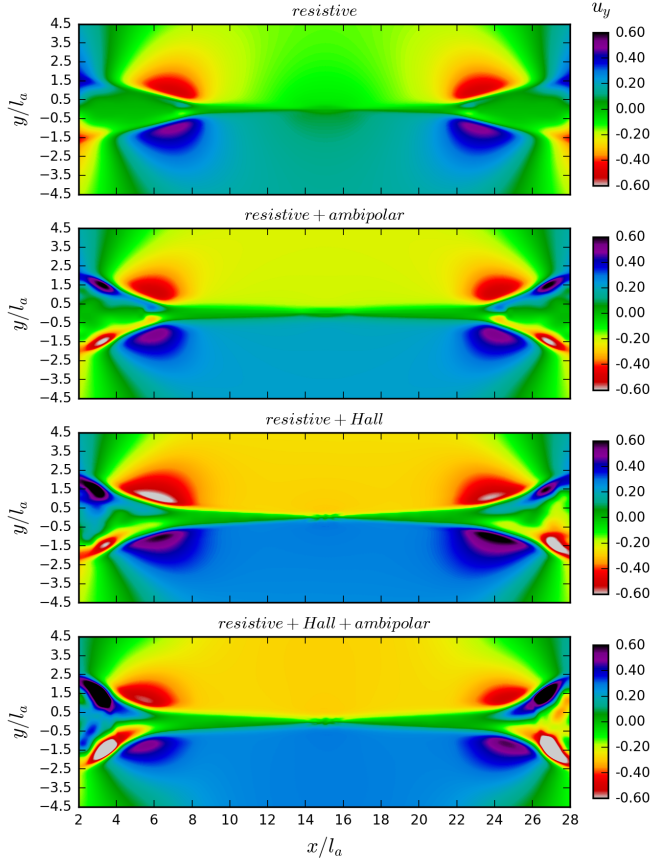


Figure 9: u_y velocity maps at $t = 12t_a$. All maps show plasma movement towards the current sheet and velocity distribution changes in its extremes. This indicates plasma is entering and exiting the diffusion region. Regions with higher velocities are found at the current sheet extremes and are highest in the presence of the Hall effect and ambipolar diffusion.

simulations is not a Sweet-Parker-type reconnection, which is not surprising since the Sweet-Parker model involves several simplifications. For example, it assumes a uniform resistivity, contrary to the localized resistivity we used for our simulations (as described in equation (37)).

Finally, concerning the formation of plasmoids, it is worth mentioning that for values of $S > 10^4$, plasmoid instability occurs Loureiro et al. (2007). In the solar chromosphere, for instance, the values of the Lundquist number are of the order of $S \sim 10^6 - 10^8$ Ni et al. (2015). Because the value we assume in our work was the critical value $S \sim 10^4$, we do not expect the formation of plasmoids.

6.3. Energy conversion and transport

Figure 11 shows the evolution of magnetic and kinetic energy measured by a detector. Similar to the reconnection rate, this detector corresponds to a point with coordinates $(N_{xi}, N_y/2, N_z/2)$, where N_{xi} is at $x = 10.0$. The results show that the kinetic energy starts from zero for the four types of simulations, in agreement with the initial data. From the initial time to $t = 5t_a$, there is a slight decrease in the magnetic energy

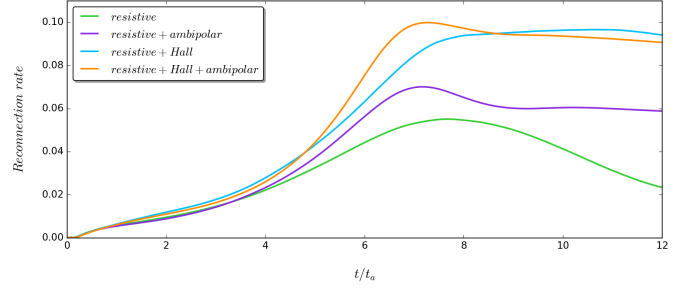


Figure 10: Reconnection rate as a function of time.

that does not lead to a noticeable increase in the kinetic energy, most likely because there is also conversion to internal energy and dissipation by Joule heating. From time $t = 5t_a$ the kinetic energy increases, coinciding with an increase in magnetic energy from $t = 5t_a$ to $t = 7t_a$. Finally, from $t = 7t_a$ to the end of the simulation, the behaviour of the curves is consistent with the reconnection process: the magnetic energy decreases while the kinetic energy increases because there is a conversion from one to the other.

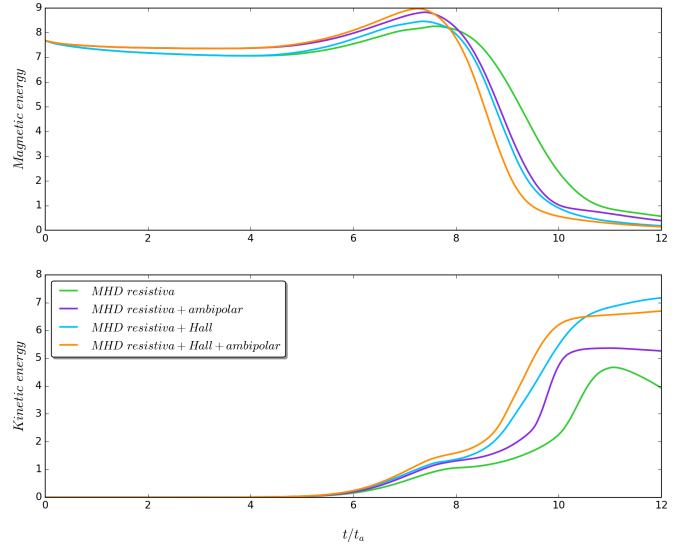


Figure 11: Temporal evolution of kinetic and magnetic energies.

The resistive+Hall and resistive+Hall+ambipolar simulations achieve the highest kinetic energy values. This suggests that the Hall and ambipolar terms not only affect the reconnection rate but also the particle acceleration. Considering that the kinetic energy of the resistive+Hall and resistive+Hall+ambipolar simulations reaches a value close to the initial value of the magnetic energy, we conclude that the Hall effect and its combination with ambipolar diffusion provide a more efficient energy conversion during the reconnection process.

To fully understand both energy conversion and transport, it is necessary to consider not only the change in energy stored in a volume but also the amount of energy flowing through the sur-

face surrounding it. In particular, we focus on a small region of the domain, including the diffusion region where reconnection occurs, and study the influence of the Hall effect and ambipolar diffusion on electromagnetic energy, bulk kinetic energy and enthalpy fluxes. The fluxes are related to the energy transport equation (5) which, in addition to describing the conservation of energy, tells us how energy is transferred from one form to another. Specifically, the electromagnetic energy flux is given by the Poynting vector $\mathbf{S} = (\mathbf{E} \times \mathbf{B})/\mu_0$, where the electric field can be obtained from Ohm's law (1). The bulk kinetic energy flux is given by $\mathbf{K} = \rho \mathbf{u}^2 \mathbf{u}/2$ and the enthalpy flux by $\mathbf{H} = (p + \rho e) \mathbf{u} = \gamma p \mathbf{u}/(\gamma - 1)$, which has a contribution from the internal energy density and another from the compressional work, $p \mathbf{u}$. These three quantities are integrated over a volume whose domain is given by $[8l_a, 16l_a] \times [-3.5l_a, 3.5l_a] \times [-0.1l_a, 0.1l_a]$. The results are shown in Figure 12, where we have plotted these fluxes as a function of time for each case, i.e. resistive, resistive+Hall, resistive+ambipolar and resistive+Hall+ambipolar.

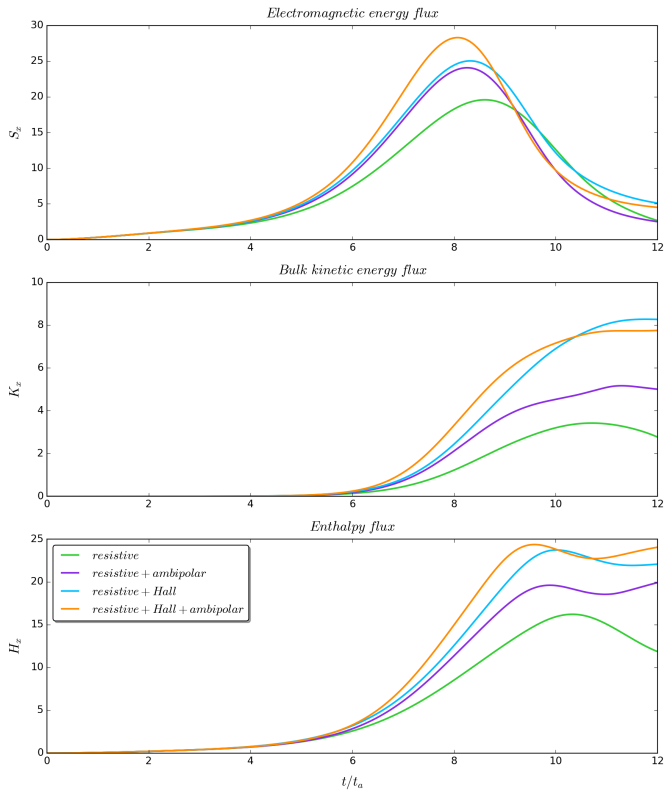


Figure 12: Temporal evolution of the electromagnetic energy flux (first panel), bulk kinetic energy flux (second panel) and enthalpy flux (third panel).

The results depicted in Figure 12 reveal that energy transport associated with reconnection primarily arises from electromagnetic and enthalpy fluxes, while kinetic energy flux plays a relatively minor role. Notably, the three panels in Figure 12 indicate that the rate of energy transfer is significantly higher in the resistive+Hall and resistive+Hall+ambipolar cases. This suggests that Hall and ambipolar effects may account for the rapid energy release during magnetic reconnection.

To quantitatively analyze this phenomenon, we measured

the increases in S_x , K_x , and H_x for the resistive+Hall, resistive+ambipolar, and resistive+Hall+ambipolar cases compared to the resistive case at time $t = 8t_a$. For S_x , we observed a 29% increase in the ambipolar case, 34% in the Hall case, and 55% in the Hall+ambipolar case. Similarly, for K_x , the increases were 73%, 99%, and 171%, respectively. Finally, for H_x , the increases were 33%, 47%, and 76%, respectively. These measurements, conducted at time $t = 8t_a$ and calculated relative to the resistive case, demonstrate that the resistive+Hall+ambipolar case exhibits the highest percentage increases, followed by the resistive+Hall case. Consequently, we can conclude that the Hall effect, particularly in combination with ambipolar diffusion, facilitates more efficient energy transport during reconnection.

7. Conclusions

Existing research has mainly focused on the Hall effect or ambipolar diffusion separately, without exploring the potential impact of their combined influence in a systematic way. In this work, we conducted a systematic study to analyze the effects of the Hall term and ambipolar diffusion on the formation and evolution of current sheets, the reconnection rate and the energy released during the magnetic reconnection process. Our findings underscore the importance of considering both effects in partially ionized plasma dynamics, where ambipolar diffusion cannot be neglected. We have observed significant enhancements in reconnection rates compared to simulations neglecting one or both processes. This integrated approach provides valuable insights into the acceleration of reconnection events in astrophysical plasmas, contributing to a more comprehensive understanding of magnetic reconnection speed-up mechanisms essential for the study of all astrophysical plasmas.

We solved the system of MHD equations with resistivity, Hall effect and ambipolar diffusion using MAGNUS. Since the code only solved the resistive MHD equations, we implemented new subroutines to calculate all terms related to the Hall effect and ambipolar diffusion in the numerical fluxes. The inclusion of these effects also required modifications to the time step. However, the presence of the Hall term in the code results in a significant reduction of the time step, which makes the execution time excessive, especially when a high spatial resolution is required.

Once the subroutines were implemented and modified, we used the initial data and boundary conditions proposed by the GEM magnetic reconnection challenge, a project to study the Hall effect in magnetic reconnection that has been used by many authors as a benchmark test. We performed four types of simulations, systematically turning on and off the Hall and ambipolar terms. Here, systematic means that the initial data, boundary conditions, computational domain, spatial resolution, and numerical methods were the same for all simulations, except for the Hall and ambipolar parameters, which changed depending on which term was turned on or off in each simulation. The four types of simulations were: resistive, resistive+Hall, resistive+ambipolar, and resistive+Hall+ambipolar.

First, we tested the Hall effect in MAGNUS by replicating the results of the GEM project. For the resistive and resistive+Hall simulations, we obtained a reconnected flux of 3.3 and 0.5, respectively, the same values as reported by Birn et al. (2001) in the GEM summary. Not only the values were the same, but also the qualitative behaviour of the curves. The same is true if we compare the results with those of other authors, such as Schmitz and Grauer (2006); Tóth et al. (2008); Strumik and Stasiewicz (2017), where only slight differences are found. Finally, since we obtained the same results as in the test, MAGNUS shows fidelity in solving the MHD equations with the Hall term.

The ambipolar diffusion term was programmed similarly to the Hall effect. No benchmark test was performed this time, but we did investigate the effect of ambipolar diffusion on the GEM problem for the first time. This was done by systematically comparing simulations where only the ambipolar parameter K_A was changed. In both the resistive+ambipolar and resistive+Hall+ambipolar simulations, the reconnected flux grows with the value of K_A . The higher value of K_A was 0.01, the less ionized case compared to the other values used in this investigation. With $K_A = 0.01$ we obtained a 75% increase of the reconnected flux for the resistive+ambipolar simulation compared to the resistive one. For the resistive+Hall+ambipolar we got a 143% increase in reconnected flux compared to the resistive+Hall simulation. However, after the increase, the flux of the latter remained quasi-stationary due to the formation of a plasmoid.

In general, the results of the GEM scenario show that the inclusion of the Hall effect produces a significant increase in the reconnected flux. Similarly, the inclusion of ambipolar diffusion produces significant increases. This suggests that ambipolar diffusion, like the Hall effect, could be one of the mechanisms for fast reconnection rates.

To study a model different from the GEM, which does not have a guide field, has uniform resistivity and has the current sheet formed since the beginning, we implemented a simple magnetic field configuration without perturbations, but with a guide-field and localized resistivity as initial data for the formation of a current sheet. In this model, the resistive+Hall+ambipolar case was the only one that reached a 0.1 value in the reconnection rate, followed by the resistive+Hall case. These results show that the Hall effect is indeed the dominant phenomenon when it comes to increasing the reconnection rate and obtaining values close to 0.1. However, ambipolar diffusion is also relevant, since it was the combination of the Hall effect and ambipolar diffusion that reached a maximum value of 0.1. Moreover, simulations with ambipolar diffusion show a faster growth of the reconnection rate, which helps explain the rapid energy release that accelerates particles.

We also found that the conversion from magnetic to kinetic energy is more efficient in the presence of the Hall effect and its combination with ambipolar diffusion. This supports the fact that both mechanisms have a significant impact on particle acceleration processes.

In addition to energy conversion, we also study its transfer through the fluxes present in the energy transport equation,

and we found that energy transport is mainly due to electromagnetic and enthalpy fluxes. The kinetic energy flux is also present but is smaller than the others. For the three fluxes, the rate of energy transfer is higher in the resistive+Hall+ambipolar case, followed by resistive+Hall and resistive+ambipolar cases. Therefore, we conclude that both mechanisms provide more efficient energy transfer, especially when combined. Since the highest energy transfer rate is for the resistive+Hall+ambipolar case, we highlight the importance of ambipolar diffusion.

Our results show that ambipolar diffusion causes magnetic energy to dissipate rapidly, facilitating the reconnection of magnetic field lines, and leading to the formation of thin current sheets. It is worth mentioning that the Hall effect enhances reconnection by altering the magnetic field topology and favouring the appearance of localized plasma current sheets, a natural outcome of the presence of a Burgers-like term. The above since the Hall term is proportional to the current, it is quadratic in \mathbf{B} , and hides a Burgers-like behaviour (Vainshtein et al., 2000)). On the other hand, the ambipolar diffusion term, which is not quadratic but cubic in \mathbf{B} , is related to a velocity in the same direction as the Lorentz force. Therefore, its effect is to dissipate the currents perpendicular to \mathbf{B} , acting to align magnetic and current fields (Viganò et al., 2019). Ambipolar effect plays a crucial role in the study of magnetic reconnection for several reasons. Mainly, it facilitates energy dissipation, which, together with the Hall effect, is essential for the optimal conversion of magnetic energy into thermal and kinetic plasma energy. The above is supported by our last results, where the rate of energy transfer shows a notable increase in the cases combining Hall and ambipolar effects.

Finally, it is essential to emphasize that although plasmas are often treated as single fluids, the distinction between ions, electrons, and neutral species becomes significant in diffusion regions where magnetic reconnection occurs. Therefore, future research should focus on a multi-species charged fluid model rather than a single-fluid approach. The different species interact through elastic and inelastic collisions. Elastic collisions involve the exchange of momentum and energy between different fluids, while inelastic collisions involve processes such as ionization and recombination. Adopting a multi-fluid approach allows for a more comprehensive study of regions within the flow sheet where turbulence is induced, such as the extremes where abrupt changes in velocity magnitude and direction occur. A recent study by Shibata et al. (2022) examined such regions in solar flares, where turbulence is also generated. A systematic study of turbulence excitation in the Earth's magnetotail using a multi-fluid framework would be very interesting and provide valuable insights. The above requires a model of the Earth's magnetotail current sheet without oversimplification.

Acknowledgements

F.D.L-C was supported by the Vicerrectoría de Investigación y Extensión - Universidad Industrial de Santander, under Grant No. 3703.

References

- Ballester, J.L., Alexeev, I., Collados, M., Downes, T., Pfaff, R.F., Gilbert, H., Khodachenko, M., Khomenko, E., Shaikhislamov, I.F., Soler, R., et al., 2018. Partially ionized plasmas in astrophysics. *Space Science Reviews* 214, 1–149.
- Bessho, N., Bhattacharjee, A., 2005. Collisionless reconnection in an electron-positron plasma. *Physical review letters* 95, 245001.
- Bessho, N., Bhattacharjee, A., 2007. Fast collisionless reconnection in electron-positron plasmas. *Physics of Plasmas* 14, 056503.
- Birn, J., Artemyev, A.V., Baker, D., Echim, M., Hoshino, M., Zelenyi, L., 2012. Particle acceleration in the magnetotail and aurora. *Space science reviews* 173, 49–102.
- Birn, J., Drake, J., Shay, M., Rogers, B., Denton, R., Hesse, M., Kuznetsova, M., Ma, Z., Bhattacharjee, A., Otto, A., et al., 2001. Geospace environmental modeling (gem) magnetic reconnection challenge. *Journal of Geophysical Research: Space Physics* 106, 3715–3719.
- Birn, J., Priest, E.R., 2007. Reconnection of magnetic fields: magnetohydrodynamics and collisionless theory and observations. Cambridge University Press.
- Bittencourt, J.A., 2013. Fundamentals of plasma physics. Springer Science & Business Media.
- Brandenburg, A., Zweibel, E.G., 1994. The formation of sharp structures by ambipolar diffusion. *Astrophysical Journal* 427, L91–L94.
- Brandenburg, A., Zweibel, E.G., 1995. Effects of Pressure and Resistivity on the Ambipolar Diffusion Singularity: Too Little, Too Late. *Astrophysical Journal* 448, 734. doi:10.1086/176001.
- Cassak, P., Liu, Y.H., Shay, M., 2017. A review of the 0.1 reconnection rate problem. *Journal of Plasma Physics* 83.
- Chen, L.J., Hesse, M., Wang, S., Gershman, D., Ergun, R., Burch, J., Bessho, N., Torbert, R., Giles, B., Webster, J., et al., 2017. Electron diffusion region during magnetopause reconnection with an intermediate guide field: Magnetospheric multiscale observations. *Journal of Geophysical Research: Space Physics* 122, 5235–5246.
- Comisso, L., Bhattacharjee, A., 2016. On the value of the reconnection rate. *Journal of Plasma Physics* 82, 595820601.
- Dahlin, J.T., Antiochos, S.K., Qiu, J., DeVore, C.R., 2022. Variability of the reconnection guide field in solar flares. *The Astrophysical Journal* 932, 94.
- Ethan, T., Lazarian, A.V., 1999. Reconnection in the interstellar medium. *The Astrophysical Journal* 511, 203.
- Falgarone, E., Momferratos, G., Lesaffre, P., 2015. The intermittency of ism turbulence: What do the observations tell us?, in: *Magnetic Fields in Diffuse Media*. Springer, pp. 227–252.
- Goodbred, M., Liu, Y.H., 2022. First-principles theory of the relativistic magnetic reconnection rate in astrophysical pair plasmas. *Physical Review Letters* 129, 265101.
- Heitsch, F., Zweibel, E.G., 2003. Fast reconnection in a two-stage process. *The Astrophysical Journal* 583, 229.
- Hesse, M., Cassak, P., 2020. Magnetic reconnection in the space sciences: Past, present, and future. *Journal of Geophysical Research: Space Physics* 125, e2018JA025935.
- Jara-Almonte, J., Ji, H., Yoo, J., Yamada, M., Fox, W., Daughton, W., 2019. Kinetic simulations of magnetic reconnection in partially ionized plasmas. *Physical review letters* 122, 015101.
- Karimabadi, H., Krauss-Varban, D., Huba, J., Vu, H., 2004. On magnetic reconnection regimes and associated three-dimensional asymmetries: Hybrid, hall-less hybrid, and hall-mhd simulations. *Journal of Geophysical Research: Space Physics* 109.
- Khomenko, E., Collados, M., 2012. Heating of the magnetized solar chromosphere by partial ionization effects. *The Astrophysical Journal* 747, 87.
- Khomenko, E., Collados, M., Diaz, A., Vitas, N., 2014. Fluid description of multi-component solar partially ionized plasma. *Physics of Plasmas* 21.
- Landinez, G., Rueda, S., Lora-Clavijo, F.D., 2021. First steps on modelling wave propagation in isotropic-heterogeneous media: numerical simulation of p–sv waves. *European Journal of Physics* 42, 065001.
- Liu, Y.H., Cassak, P., Li, X., Hesse, M., Lin, S.C., Genestreti, K., 2022. First-principles theory of the rate of magnetic reconnection in magnetospheric and solar plasmas. *Communications Physics* 5, 97.
- Lora-Clavijo, F., Cruz-Osorio, A., Guzmán, F., 2015. Cafe: a new relativistic mhd code. *The Astrophysical Journal Supplement Series* 218, 24.
- Loureiro, N., Schekochihin, A.A., Cowley, S.C., 2007. Instability of current sheets and formation of plasmoid chains. *Physics of Plasmas* 14.
- Malyshkin, L.M., Zweibel, E.G., 2011. Onset of fast magnetic reconnection in partially ionized gases. *The Astrophysical Journal* 739, 72.
- Morales, P.A.G., 2020. Modeling of non-ideal magnetohydrodynamic effects in the solar atmosphere. Ph.D. thesis. Universidad de La Laguna (Islas Canarias, España).
- Nakamura, T.K., Genestreti, K., Liu, Y.H., Nakamura, R., Teh, W.L., Hasegawa, H., Daughton, W., Hesse, M., Torbert, R., Burch, J., et al., 2018. Measurement of the magnetic reconnection rate in the earth’s magnetotail. *Journal of Geophysical Research: Space Physics* 123, 9150–9168.
- Navarro, A., Lora-Clavijo, F., González, G.A., 2017. Magnus: a new resistive mhd code with heat flow terms. *The Astrophysical Journal* 844, 57.
- Navarro, A., Lora-Clavijo, F., Murawski, K., Poedts, S., 2021. Thermal conduction effects on formation of chromospheric solar tadpole-like jets. *Monthly Notices of the Royal Astronomical Society* 500, 3329–3334.
- Navarro, A., Murawski, K., Wójcik, D., Lora-Clavijo, F., 2019. Numerical simulations of the emerging plasma blob into a solar coronal hole. *Monthly Notices of the Royal Astronomical Society* 489, 2769–2774.
- Ni, L., Kliem, B., Lin, J., Wu, N., 2015. Fast magnetic reconnection in the solar chromosphere mediated by the plasmoid instability. *The Astrophysical Journal* 799, 79.
- Nóbrega-Siverio, D., Martínez-Sykora, J., Moreno-Insertis, F., Carlsson, M., 2020. Ambipolar diffusion in the bifrost code. *Astronomy & Astrophysics* 638, A79.
- Parker, E.N., 1957. Sweet’s mechanism for merging magnetic fields in conducting fluids. *Journal of Geophysical Research* 62, 509–520.
- Parker, E.N., 1963. The solar-flare phenomenon and the theory of reconnection and annihilation of magnetic fields. *The Astrophysical Journal Supplement Series* 8, 177.
- Price, L., Swisdak, M., Drake, J.F., Cassak, P., Dahlin, J., Ergun, R., 2016. The effects of turbulence on three-dimensional magnetic reconnection at the magnetopause. *Geophysical Research Letters* 43, 6020–6027.
- Priest, E., Forbes, T., 2000. Magnetic reconnection. Cambridge University Press.
- Pritchett, P., 2001. Geospace environment modeling magnetic reconnection challenge: Simulations with a full particle electromagnetic code. *Journal of Geophysical Research: Space Physics* 106, 3783–3798.
- Schiesser, W.E., Griffiths, G.W., 2009. A compendium of partial differential equation models: method of lines analysis with Matlab. Cambridge University Press.
- Schmitz, H., Grauer, R., 2006. Kinetic vlasov simulations of collisionless magnetic reconnection. *Physics of plasmas* 13, 092309.
- Schnack, D.D., 2009. Lectures in magnetohydrodynamics: with an appendix on extended MHD. Springer.
- Shen, C., Chen, B., Reeves, K.K., Yu, S., Polito, V., Xie, X., 2022. The origin of underdense plasma downflows associated with magnetic reconnection in solar flares. *Nature Astronomy* 6, 317–324.
- Shibata, K., Takasao, S., Reeves, K.K., 2022. Numerical study on excitation of turbulence and oscillation in above-the-loop-top region of a solar flare. arXiv preprint arXiv:2212.05802.
- Singh, K., Sakaue, T., Nakamura, N., Kawamura, A.D., Isobe, H., Shibata, K., 2019. Effect of ionization and recombination on the evolution of the harristype current sheet in partially ionized plasmas. *The Astrophysical Journal* 884, 161.
- Strumik, M., Stasiewicz, K., 2017. Multidimensional hall magnetohydrodynamics with isotropic or anisotropic thermal pressure: Numerical scheme and its validation using solitary waves. *Journal of Computational Physics* 330, 846–862.
- Sweet, P., 1958a. The production of high energy particles in solar flares. *Il Nuovo Cimento (1955-1965)* 8, 188–196.
- Sweet, P.A., 1958b. The neutral point theory of solar flares, in: *Electromagnetic phenomena in cosmical physics*, p. 123.
- Tóth, G., Ma, Y., Gombosi, T.I., 2008. Hall magnetohydrodynamics on block-adaptive grids. *Journal of Computational Physics* 227, 6967–6984.
- Uzdensky, D.A., Kulsrud, R.M., 2006. Physical origin of the quadrupole out-of-plane magnetic field in hall-magnetohydrodynamic reconnection. *Physics of Plasmas* 13.
- Vainshtein, S., Chitre, S., Olinto, A., 2000. Rapid dissipation of magnetic fields due to the hall current. *Physical Review E* 61, 4422.
- Viganò, D., Martínez-Gómez, D., Pons, J.A., Palenzuela, C., Carrasco, F., Miñano, B., Arbona, A., Bona, C., Massó, J., 2019. A simflowny-based high-performance 3d code for the generalized induction equation. *Computer*

Physics Communications 237, 168–183.

Wandurraga, P.C., Navarro, A., Lora-Clavijo, F.D., 2021. Torsional alfvén waves propagation in a stratified solar atmosphere. *Revista de la Academia Colombiana de Ciencias Exactas, Físicas y Naturales* 45, 52–66.

Zaqarashvili, T.V., Khodachenko, M.L., Rucker, H.O., 2011. Magnetohydrodynamic waves in solar partially ionized plasmas: two-fluid approach. *Astronomy and Astrophysics* 529, A82. doi:10.1051/0004-6361/201016326, arXiv:1101.3913.

Zweibel, E.G., 2015. Ambipolar diffusion, in: *Magnetic Fields in Diffuse Media*. Springer, pp. 285–309.

Zweibel, E.G., Yamada, M., 2009. Magnetic reconnection in astrophysical and laboratory plasmas. *Annual review of astronomy and astrophysics* 47, 291–332.